

Cite this: *J. Mater. Chem. C*,
2024, 12, 7909

Mixed ionic-electronic conduction in Ruddlesden–Popper and Dion–Jacobson layered hybrid perovskites with aromatic organic spacers†

Algirdas Dučinskas,^{ab} Mina Jung,^b Ya-Ru Wang,^{ib} Jovana V. Milić,^{id}*^{ac}
Davide Moia,^{ib}*^b Michael Grätzel,^{ib}*^a and Joachim Maier,^{id}*^b

The understanding of mixed ionic-electronic conductivity in hybrid perovskites has enabled major advances in the development of optoelectronic devices based on this class of materials. While recent investigations revealed the potential of using dimensionality effects for various applications, the implication of this strategy on mixed conductivity is yet to be established. Here, we present a systematic analysis of mixed conduction in layered (2D) hybrid halide perovskite films based on 1,4-phenylenedimethylammonium (PDMA) and benzylammonium (BzA) organic spacers in (PDMA)PbI₄ and (BzA)₂PbI₄ compositions, forming representative Dion–Jacobson (DJ) and Ruddleson–Popper (RP) phases, respectively. Electrochemical measurements of charge transport parallel to the layered structure reveal mixed ionic-electronic conduction with electronic transport mediated by electron holes in both DJ and RP phases. In comparison to the 3D perovskites, larger activation energies for both ionic and electronic conductivities are observed which result in lower absolute values. While the layered perovskites still allow for a relatively efficient exchange of iodine with the gas phase, the lower change of conductivity on the variation of the iodine partial pressure compared with 3D perovskites is consistent with the exchange affecting only a fraction of the film, with implications for the encapsulating efficacy of these materials. We complement the analysis with a demonstration of the superior thermal stability of DJ structures compared to their RP counterparts. This can guide future explorations of dimensionality and composition to control the transport and stabilization properties of 2D perovskite films.

Received 14th March 2024,
Accepted 29th April 2024

DOI: 10.1039/d4tc01010h

rsc.li/materials-c

Introduction

Ion migration is a determining factor for the stability and performance of metal halide perovskites,^{1–5} enabling the design of devices with novel functionalities.^{4,6–9} While the role of ion transport in the electrical response of perovskite solar cells is still a matter of debate, the general consensus is that reducing or suppressing ion migration in these devices would be beneficial for their long-term operational stability.^{3–5} Compositional engineering can, to an extent, reduce the problem of ion migration. For example, partial substitution of A-cations in methylammonium (MA) lead iodide (MAPbI₃) compositions has been shown to increase the activation energy for the

migration of halide vacancies, which are majority carriers in these systems.¹⁰ Varying the dimensionality could provide a more effective way to tailor ionic transport.^{11–13} Hybrid perovskite materials with reduced dimensionality are templated by large organic spacer cations (S), which could act as intrinsic barriers preventing ion migration. They form 2D perovskite structures, which are typically based on S_xA_{n–1}M_nX_{3n+1} compositions, where A is a central cation (*e.g.*, MA, Cs, or formamidine), M divalent metal (mostly Pb²⁺ or Sn²⁺), X halide anion (I[–], Br[–], or Cl[–]), and S either mono- (*x* = 2) or divalent (*x* = 1) alkylammonium spacer cations. The spacers template corner-sharing {MX₆} octahedral slabs with perovskite structures that form RP and DJ phases. These are primarily determined by the structure of spacer cations (Fig. 1a),^{14–18} which is also expected to affect the ionic transport properties. For instance, it has been shown that the spacer moieties have a significant role in controlling photo-induced halide segregation, which is directly related to ion migration.^{19–21} Moreover, layered perovskites based on *n*-butylammonium (BA) spacers are reported to feature suppressed ion migration along the in-plane direction.^{12,13} Similarly, systems based on 2-phenylethylammonium (PEA)

^a Laboratory of Photonics and Interfaces, École Polytechnique Fédérale de Lausanne, 1015 Lausanne, Switzerland. E-mail: michael.gratzel@epfl.ch

^b Max Planck Institute for Solid State Research, Heisenbergstr. 1, 70569 Stuttgart, Germany. E-mail: d.moia@fkf.mpg.de, office-maier@fkf.mpg.de

^c Adolphe Merkle Institute, University of Fribourg, 1700 Fribourg, Switzerland. E-mail: jovana.milic@unifr.ch

† Electronic supplementary information (ESI) available. See DOI: <https://doi.org/10.1039/d4tc01010h>





Fig. 1 (a) Schematic of RP (top) and DJ (bottom) phases in this study with the corresponding (BzA, PDMA) spacer structures (cyan) and different alignments between the adjacent inorganic layers (blue). (b) X-ray diffraction patterns of $(\text{BzA})_2\text{PbI}_4$ (blue) and $(\text{PDMA})\text{PbI}_4$ (black). Here * corresponds to higher-order ($h00$) reflections.^{24–28} UV-vis absorption spectra of the films are shown in Fig. S1 (ESI†) with XRD patterns showing comparable structures of the materials in films and devices (ESI†). (c) Schematic representation of the electrode substrate (quartz) used for electrical measurements. Inset: Graphic illustration of a DJ perovskite placed between two electrodes. (d) SEM images of $(\text{PDMA})\text{PbI}_4$ and $(\text{BzA})_2\text{PbI}_4$ thin films deposited on the substrates with interdigitated contacts (5 μm wide gold fingers are visible in the image). Insets represent the SEM images of the films at higher magnification (the corresponding scale bars are shown on the images).

spacers were found to have a high activation energy for ion migration.²² Such previous reports mostly involve the analysis of the ionic properties of 2D perovskites based on monofunctional spacers, which typically form RP perovskite structures. However, DJ perovskites employing bifunctional spacers are of increasing interest for optoelectronic applications,^{23–29} especially considering their high thermal stability.²⁹ However, their mixed ionic-electronic conductivity in comparison with RP analogs is not well understood. In particular, the effect of the reduced interlayer spacing and the lack of the van der Waals gap in DJ phases on their ionic and electronic transport requires clarification.

In this work, we investigate the electrochemical response of RP and DJ layered hybrid perovskite model systems based on comparable aromatic spacer moieties, namely benzylammonium (BzA) and 1,4-phenylenedimethylammonium (PDMA) in $(\text{BzA})_2\text{PbI}_4$ and $(\text{PDMA})\text{PbI}_4$ compositions, respectively. We apply electrochemical techniques to elucidate the effect of dimensionality and interlayer spacing on mixed conductivity in layered hybrid perovskites of interest to optoelectronics.

Results

This study focuses on representative layered hybrid perovskites based on $n = 1$ compositions comprising BzA, which crystallize in RP type $(\text{BzA})_2\text{PbI}_4$ structure, and PDMA spacers, forming DJ $(\text{PDMA})\text{PbI}_4$ perovskites (Fig. 1a and b).^{24–28} The preparation is detailed in the Methods section of the ESI.†

The structural properties of thin films were investigated by X-ray diffraction (XRD, Fig. 1b). XRD patterns of a $(\text{BzA})_2\text{PbI}_4$

thin film deposited on glass substrates show $(00l)$ reflection peaks, which indicate the presence of crystallites with perovskite layers that are oriented parallel to the substrate. Similarly, the most intense peaks of $(\text{PDMA})\text{PbI}_4$ films show $(h00)$ Miller indices corresponding to the parallel orientation of perovskite layers with respect to the substrate (Fig. 1b). In addition, there are $(0kl)$ reflections coming from perpendicularly orientated perovskite layers with lower intensity, implying that the dominant crystallite orientation is parallel to the substrate with a larger d -spacing for RP as compared to DJ phases.²⁶ The spacers affect the domain sizes for the corresponding phases in thin films with dimensions in the order of 10–20 μm for DJ and hundreds of nanometres for the RP thin films.^{24–30} This is relevant for the electrochemical measurements, which were based on the device architecture with interdigitated gold contacts (Fig. 1c). Considering the preferential orientation of the crystallites,^{24–28} the in-plane conductivity is expected to dominate the measured response (Fig. 1c, inset). The films deposited on quartz substrates with interdigitated gold contacts were assessed by scanning electron microscopy (SEM), evidencing that both $(\text{PDMA})\text{PbI}_4$ and $(\text{BzA})_2\text{PbI}_4$ (Fig. 1d) feature compact uniform morphology.

The electrical properties were measured by galvanostatic polarization and impedance spectroscopy experiments (detailed in the Methods section). Direct current (DC) measurements performed in an argon atmosphere at 60 °C in the dark display significant polarization in the thousands of seconds timescale, as evidenced by the increase in measured voltage as a function of time for $(\text{PDMA})\text{PbI}_4$ and $(\text{BzA})_2\text{PbI}_4$ films (Fig. 2). This observation is consistent with a significant ionic conductivity, similar to previous results obtained for 3D perovskites.^{31–35} The electronic conductivity extracted from the long time scale resistance, assuming ion-blocking behaviour at the perovskite-gold interface, is on the order of $2\text{--}5 \times 10^{-11} \text{ S cm}^{-1}$ for both DJ and RP systems.^{24–28} Accurate evaluation of the ionic conductivity



Fig. 2 Galvanostatic polarization measurements performed on horizontal devices with (a) $(\text{PDMA})\text{PbI}_4$ and (b) $(\text{BzA})_2\text{PbI}_4$ thin films in an argon atmosphere and under iodine atmosphere ($P(\text{I}_2) = 7 \times 10^{-7} \text{ bar}$; argon carrier gas) at 60 °C in the dark. Impedance spectra collected under analogous conditions are shown in (c) for the DJ and (d) for the RP film.



is challenging under these conditions; the impedance spectra do not show a clear high-frequency feature, complicating the fit of equivalent circuit models.^{34,35} We estimate upper limits to the ionic conductivity in the range of 10^{-11} – 10^{-10} S cm⁻¹ by fitting both bulk and grain boundary elements (two R-C in series) to the high-frequency feature of the impedance to extract the total conductivity. We also account for the analysis of the gap width L (Fig. 1c) dependence of the electrical response for these estimates.³⁴ This highlights the presence of an interfacial resistance for the DJ film measured under argon, which becomes negligible when the sample is measured under fixed iodine partial pressure ($P(I_2)$) (see Supplementary discussion and Fig. S2, ESI†). We can, thus, confidently assign such estimates to the bulk properties.

Dimensionality reduction has a clear and substantial effect on electrical properties, in that both RP and DJ samples have several orders of magnitude lower electronic conductivities (σ_{eon}) in the dark in comparison to MAPbI₃, for which values on the order of 10^{-9} – 10^{-6} S cm⁻¹ were previously reported.^{11,32–37} The lower electronic conductivity of layered hybrid perovskites is likely due to their larger bandgap and charge carrier confinement, which could further decrease the concentration of electronic charge carriers. These effects would be lower in quasi-2D perovskites based on nominal compositions with $n > 1$, as their structural and optoelectronic properties approach those of 3D perovskites. The reduced ionic conductivity could also be associated with multiple factors, including defect formation energy, anisotropy effects, or ion migration energy barrier, which will be discussed later.

The conductivity of mixed conductors can be modulated by changing their stoichiometry *in situ*. This has been experimentally demonstrated for hybrid perovskites by measuring their electrical properties under fixed iodine partial pressure.² When RP and DJ samples are exposed to iodine partial pressure (7×10^{-7} bar), changes in the polarization curves and in the shape of the impedance spectra of both (PDMA)PbI₄ (Fig. 2a and c) and (BzA)₂PbI₄ (Fig. 2b and d) are evidenced compared to the argon case. As a result, larger values of the electronic conductivity and shorter time constants in the DC measurements are found for the high $P(I_2)$. To probe the conduction type and gain insights into the defect chemistry of these systems, partial conductivities in (PDMA)PbI₄ and (BzA)₂PbI₄ are analysed as a function of iodine partial pressure, in the range from 3.5×10^{-7} to 1.4×10^{-5} bar (Fig. 3a and b), using DC and AC measurements performed after equilibration at each condition. Upon increasing iodine partial pressure, the electronic conductivity increases with a slope of approximately 0.5–0.6 in both RP and DJ compounds (dashed lines in Fig. 3a and b), indicating a p-type character for the electronic conduction.³⁶ Such change in conductivity is only partially reversible, as highlighted by the data points referring to the first scan. Specifically, a larger value of σ_{eon} is retained when returning the initial $P(I_2)$ value. When performing a second forward and reverse scan in $P(I_2)$, we find a much more reversible trend of the electronic conductivity, however with a reduced slope of 0.35–0.4, for both samples (see protocol for



Fig. 3 (a) and (b) Electronic and ionic conductivities of (a) (PDMA)PbI₄ and (b) (BzA)₂PbI₄. The positive slope of σ_{ion} vs. $P(I_2)$ recorded for the RP film points to possible inaccuracy in its estimation (see text). (c) and (d) Electronic conductivity as a function of time extracted from a series of DC polarization measurements performed during the equilibration of (PDMA)PbI₄ and of (BzA)₂PbI₄ based devices when $P(I_2)$ is adjusted from 1.3×10^{-7} to 1.3×10^{-6} bar and when the reverse step is applied. The carrier gas is argon and the sample temperature 60 °C. (e) and (f) Arrhenius plots of (PDMA)PbI₄ (e) and (BzA)₂PbI₄ (f) for electronic (eon, black) and ionic (ion, red) charge carrier transport obtained from conductivity measurements performed in the dark under $P(I_2) 6.9 \times 10^{-7}$ bar atmosphere. In the legend label, an upward and a downward arrow are used to indicate the temperature scan used for collecting the data points to describe the increasing and decreasing temperature, respectively.

the experiment in the Methods section of the ESI†). Such observation could be consistent with some reactivity of the sample to iodine that irreversibly changes its properties. The ionic conductivities of the two thin films undergo a less pronounced change when varying $P(I_2)$, with a slight decrease for the DJ sample and a more significant increase for the RP sample. The overall slopes recorded for the ionic conductivities of the DJ and RP samples are on the order of -0.16 and 0.33 , respectively. We expect a large error associated with the estimated ionic conductivity. For the DJ sample, the slightly negative slope extracted for the ionic conductivity data is consistent with the intrinsic behaviour of the film and provides confidence in the interpretation of the data. On the other hand, the positive slope extracted for the RP sample cannot be easily explained and it might point to a more complex electronic and ionic transport mechanism in the film, and accordingly, to a possible overestimation of the ionic conductivity in our analysis



(further discussion on possible defect chemical models relevant to these 2D systems can be found in the Sections 2 and 3 of the ESI†).

The kinetics of iodine exchange with the films was analyzed to probe the effect of dimensionality reduction on the incorporation/excorporation of halogen. The evolution in the electronic conductivity as a function of time after switching the iodine partial pressure in the measuring cell was recorded by performing a sequence of DC polarization measurements. Even though layered perovskites are more resistive than MAPbI₃ and iodine incorporation is expected to occur across layers separated by insulating organic spacers in the sample architecture used (Fig. 1c), the equilibration kinetics show a relatively short characteristic time constant of 2–10 h (Fig. 3c and d, data fitted with a single exponential function; fit of a double exponential also shown for the iodine excorporation). Note that the differences in time constant between the incorporation and excorporation reactions can be explained by the relatively large steps in $P(I_2)$ value used here. These were selected to detect large enough changes in conductivity. The time scale of the iodine exchange, which is comparable to the one recorded for MAPbI₃ under similar conditions,³⁸ would not point to bulk diffusion as a limiting factor to the overall reaction. It is possible that in the 2D systems, the surface exchange may be the limiting step to the exchange reaction,³⁹ although anisotropy effects make the comparison with the polarization timescale difficult. It is also interesting that similar kinetics recorded for DJ and RP samples refer to two different film compositions but also different surface morphologies. The relatively efficient surface reaction step in the studied DJ and RP systems points to the possible diffusion of iodine within the perovskite layers, such as through grain boundaries and other high dimensional defects in the films (Fig. S3, ESI†), as well as in regions where layer orientations that are not parallel to the substrate are present, which may be more likely for DJ films. The observed halogen exchange at the solid/gas interface for both RP and DJ films could potentially undermine their use for passivation in perovskite solar cells. As noted above, it is striking that the $P(I_2)$ dependence of the electronic conductivity in these films is less pronounced than the one reported for MAPbI₃ after exposure to large iodine partial pressures (in the intrinsic region, $\sigma \propto P(I_2)^{1/2}$, see Section 4 of the ESI†). Indeed, if some parts of the films (possibly the region far from the solid–gas interface) were less accessible due to the layered nature of the compounds, the exchange of iodine would induce a <1/2 slope in the conductivity trend vs. $P(I_2)$. As a result, such “retardation” in iodine exchange would provide an enhanced encapsulation capability, compared with the case of a 3D perovskite film that is fully exposed to the gas phase, while not entirely resolving the issue of halogen exchange. Future investigations are needed to ascertain such a scenario.

To assess the activation energies for ion migration, we analysed the temperature dependence of the ionic and electronic conductivities based on the relation in eqn 1.

$$\sigma(T) = \frac{\sigma_0}{T} \exp\left(\frac{-E_a}{kT}\right) \quad (1)$$

here, σ_0 is a prefactor, k is Boltzmann constant, E_a is the activation energy, and T is the temperature in Kelvin. Because of the different annealing temperatures (*i.e.*, 100 °C (BzA)₂PbI₄ and 150 °C (PDMA)PbI₄), the DJ film was measured in the range between 333 and 393 K, while the RP film from 323 K to 353 K. The activation energies of the electronic and ionic conductivity in (PDMA)PbI₄ extracted from upward and downward temperature scans are in the order of 0.4 to 0.5 eV for $E_{a, \text{eion}}$ and 0.84 for $E_{a, \text{ion}}$, respectively (Fig. 3e). A slight decrease in magnitude is observed for the latter compared to the former scan for both electronic and ionic conductivities. These activation energy values are larger than values reported for 3D perovskites. The larger $E_{a, \text{eion}}$ is consistent with their larger bandgap and deeper valence band edge compared to 3D iodide perovskites.^{1,4,40,41} In contrast, the large value of $E_{a, \text{ion}}$ may be due to a larger defect formation energy, although changes in migration energy and possible contribution from grain boundaries cannot be excluded. The conductivity for the RP sample underwent clear changes during the temperature-dependent measurements. We recognize two different slopes for both the electronic and ionic conductivity in the Arrhenius plot (Fig. 3f). While relatively small E_a are recorded for the increasing temperature scan, much larger E_a and lower conductivities are extracted when decreasing temperature, suggesting irreversible changes occurring under these conditions (Fig. S4, ESI†). The slightly larger E_a for (PDMA)PbI₄ compared with typical values reported for 3D perovskites might also be attributed to a higher degree of octahedral distortion.⁴² Moreover, while the accumulation of ionic defects at grain boundaries would enhance conductivity and potentially lower the activation energy,⁴³ our data point to the blocking of grain boundaries in the (PDMA)PbI₄ film (Fig. S2 and ESI†). Since the data in (Fig. 3e) were collected for a device with gap width of 10 μm (shorter than the average grain size), such blocking behaviour is not expected to influence significantly the measured E_a . On the other hand, anisotropy effects due to layered crystal structure have to be taken into account. In this regard, E_a across perovskite layers may be affected by the orientation. Thus, the E_a of (PDMA)PbI₄ might be influenced by crystallites with the perovskite basal planes perpendicular to the substrate and intra-grain misorientation, as well as shorter interlayer distances between adjacent inorganic slabs as compared to RP phases. The (BzA)₂PbI₄ RP sample consists of crystallites with layer orientation parallel to the substrate, allowing, in principle, to measure in-plane activation energy. Irreversibility in the temperature-dependent conductivity did not allow for reliable E_a measurements. Attempts to record the out-of-plane activation energy were unsuccessful since there is no strategy to effectively control the crystal orientation at this point. Direct electrode deposition on top of perovskites also did not yield measurable devices. For this purpose, measurements on single crystals might be a good alternative in the future. Nevertheless, our data reveal that, for DJ samples, layered hybrid perovskites have higher E_a of ionic transport as compared to their 3D counterparts, confirming that dimensionality reduction is an effective strategy to mitigate ion migration. Previous studies report activation energies



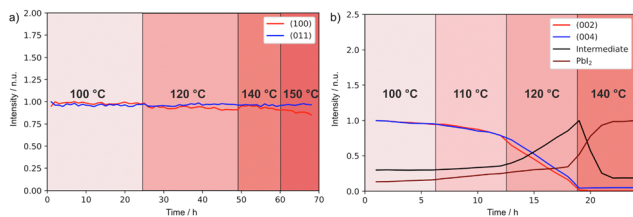


Fig. 4 XRD peak intensity change over time and of (a) (PDMA)PbI₄ sample in the temperature range of 100–150 °C and of (b) (BzA)₂PbI₄ sample in the temperature range of 100–140 °C in a nitrogen atmosphere. The peak intensities were normalized by taking the initial values at starting temperatures (Fig. S6c, ESI†).

of iodide defects in MAPbI₃ in the range 0.2–0.6 eV.^{32,41,44–47} These values are very dispersed because activation energy depends on several parameters, and in particular, the specific defect chemical situation resulting from the preparation step.⁴⁸ Specifically, variations in the local structure might significantly affect the activation energy barrier. For instance, it has been shown that partial A cation substitution could result in increased,^{10,49} or decreased E_a .⁵⁰ In addition, morphology is also an essential factor affecting activation energy, as grain boundaries might facilitate or hinder ion transport.⁴³ Lastly, dimensionality reduction has been proven an effective strategy to increase activation energy. More specifically, suppressed ion migration along the in-plane direction has been reported in (BA)₂(MA)₂Pb₃I₁₀,¹³ while others have shown 0.74 eV activation energy in (PEA)₂Pb(Br,I)₄ thin films.²²

To gain further insights into the effects on the thermal stability of these 2D materials, which is relevant to their application,²⁹ DJ and RP thin films were analysed using *in situ* temperature-dependent XRD in the dark under a nitrogen atmosphere. By tracking the intensities of diffraction peaks over time (Fig. 4a and b) we reveal that (BzA)₂PbI₄ (002) and (004) peaks slightly change at 90–100 °C, indicating minor layered structure disruption in this temperature range (Fig. S6a, ESI†). Moreover, a peak at 6.9° appears during the measurement and becomes more intense with time, which we interpret in terms of layered structure conversion to another intermediate phase occurring for the BzA-based RP sample for temperatures greater than ~90 °C (Fig. S6c, ESI†). At higher temperatures, this phase is transformed into PbI₂ (Fig. 4b). We note that (BzA)₂PbI₄ films show no decomposition (Fig. S6b, ESI†) when kept at 60 °C for up to 42 days, indicating that no significant structural changes occurred during the electrical characterization performed at such temperature.⁴⁴ We note that temperature stability of the RP film would be expected in the temperature range used to collect the data (Fig. 3f, 50–80 °C) based on this analysis. The recorded irreversible conductivity trend points to changes in the material occurring already at temperatures in the order of 80 °C, which are however not detectable from our XRD study. Importantly, the data (Fig. 3f) were collected under a fixed $P(I_2)$, which may lead to slight differences in the thermochemical stability of the material. On the contrary, the (PDMA)PbI₄ samples show remarkably better thermal stability as no degradation is observed in the

temperature range up to 150 °C (Fig. 4a and Fig. S6d, ESI†), corroborating enhanced stabilities of DJ as compared to RP phases.

This difference in thermal stability between the DJ and the RP compounds can be related to the van der Waals gap between organic layers in RP hybrid halide perovskites. Weakly bound spacer molecules might be more susceptible to thermal stress, which could eventually induce material degradation. In contrast, bifunctional spacers in DJ analogues do not form a van der Waals gap between adjacent perovskite layers, thereby featuring shorter I··I interlayer distances, which can be relevant for their thermal stability.²⁹ Consequently, the more rigid structure provides improved stability at high temperatures^{26,29,51} as corroborated by the results. This makes DJ perovskites potentially more promising materials for designing protection and passivation layers in perovskite solar cells.

Conclusions

We investigate the electrochemical properties of (PDMA)PbI₄ and (BzA)₂PbI₄ layered perovskite thin films representing DJ and RP phases, respectively. We find that these materials are mixed ionic-electronic conductors, with ionic conductivities on the order of 10⁻¹⁰ S cm⁻¹ in the dark close to equilibrium at 60 °C in the direction parallel to the perovskite layers, about 2–4 orders of magnitude lower compared to 3D hybrid perovskites. This result emphasizes the lowering of ion transport by dimensional reduction. The similar conductivity values measured for DJ and RP samples indicate that the chemical nature of the spacer is of minor influence on the conduction properties. Exposure of the samples to atmospheres with fixed iodine partial pressure revealed iodine incorporation and excorporation rates comparable to MAPbI₃. Increased electronic conductivity on increasing iodine partial pressure indicates p-type conduction in both the RP and DJ systems. Temperature-dependent conductivity measurements indicate higher activation energies of ion migration in the 2D phases compared to 3D hybrid perovskites, consistent with the suppressed ionic conductivity. We demonstrated thermal stability up to 150 °C for (PDMA)PbI₄ DJ samples. This is not matched by (BzA)₂PbI₄ films, which suffer from degradation detected with XRD measurements at temperatures above ~100 °C, and irreversible changes in conductivity already at temperatures ~80 °C. This is possibly due to weak van der Waals interactions in the spacer layer. We conclude that, despite their significantly reduced ion migration compared to 3D systems, layered perovskite compositions based on phenyl-derived aromatic spacers still allow for detectable halogen exchange with the gas phase. While these findings partially challenge the current perspective on the role of these materials in stabilizing perovskite devices, they stimulate further investigations to realize their potential through a careful understanding of layer stacking and surface reactions. These questions may become more critical for quasi-2D perovskites ($n > 1$) due to inherited features from 3D perovskites, with broad implications in perovskite materials and devices.

Author contributions

The manuscript was written by A. D. with the support of D. M. and J. V. M., whereas J. V. M., M. G. and J. M. conceptualized



the study. A. D. prepared the samples and conducted the analysis with the support of D. M., Y.-R. W. and M. J. while J. V. M. and D. M. supervised A. D., and J. M. and M. G. directed the project. All authors have approved the final manuscript.

Data availability

Data can be accessed at the DOI:10.5281/zenodo.11123730 and it is available under the license CC-BY-4.0.

Conflicts of interest

There are no conflicts to declare. Open Access funding provided by the Max Planck Society.

Acknowledgements

A. D., D. M., J. M. and M. G. acknowledge the support from the Max Planck Society and the Max-Planck/EPFL Center. J. V. M. is grateful for the Swiss National Science Foundation grant no. 193174.

Notes and references

- W. Tress, *J. Phys. Chem. Lett.*, 2017, **8**, 3106–3114.
- A. Senocrate and J. Maier, *J. Am. Chem. Soc.*, 2019, **141**, 8382–8396.
- R. Wang, M. Mujahid, Y. Duan, Z.-K. Wang, J. Xue and Y. Yang, *Adv. Funct. Mater.*, 2019, **29**, 1808843.
- M. H. Futscher and J. V. Milić, *Front. Energy Res.*, 2021, **9**, 629074.
- J. Bisquert and E. J. Juarez-Perez, *J. Phys. Chem. Lett.*, 2019, **10**, 5889–5891.
- A. Enocrate, E. Kotomin and J. Maier, *Helv. Chim. Acta*, 2020, **103**, e2000073.
- Y. Park and J.-S. Lee, *J. Phys. Chem. Lett.*, 2022, **13**, 5638–5647.
- K. Sakhatskyi, R. A. John, A. Guerrero, S. Tsarev, S. Sabisch, T. Das, G. J. Matt, S. Yakunin, I. Cherniukh, M. Kotyrba, Y. Berezovska, M. I. Bodnarchuk, S. Chakraborty, J. Bisquert and M. V. Kovalenko, *ACS Energy Lett.*, 2022, **10**, 3401–3414.
- J. Bisquert and A. Guerrero, *J. Phys. Chem. Lett.*, 2022, **13**, 3789–3795.
- D. W. Ferdani, S. R. Pering, D. Ghosh, P. Kubiak, A. B. Walker, S. E. Lewis, A. L. Johnson, P. J. Baker, M. S. Islam and P. J. Cameron, *Energy Environ. Sci.*, 2019, **12**, 2264–2272.
- Y. Yuan and J. Huang, *Acc. Chem. Res.*, 2016, **49**, 286–293.
- Y. Lin, Y. Bai, Y. Fang, Q. Wang, Y. Deng and J. Huang, *ACS Energy Lett.*, 2017, **2**, 1571–1572.
- X. Xiao, J. Dai, Y. Fang, J. Zhao, X. Zheng, S. Tang, P. N. Rudd, X. C. Zeng and J. Huang, *ACS Energy Lett.*, 2018, **3**, 684–688.
- D. B. Mitzi, *J. Chem. Soc., Dalton Trans.*, 2001, **1**, 1–12.
- B. Saparov and D. B. Mitzi, *Chem. Rev.*, 2016, **116**, 4558–4596.
- G. Grancini and M. K. Nazeeruddin, *Nat. Rev. Mater.*, 2019, **4**, 4–22.
- L. Mao, S. M. L. Teicher, C. C. Stoumpos, R. M. Kennard, R. A. DeCrescent, G. Wu, J. A. Schuller, M. L. Chabinyc, A. K. Cheetham and R. Seshadri, *J. Am. Chem. Soc.*, 2019, **141**, 19099–19109.
- X. Li, J. M. Hoffman and M. G. Kanatzidis, *Chem. Rev.*, 2021, **121**, 2230–2291.
- P. S. Mathew, J. T. DuBose, J. Cho and P. V. Kamat, *ACS Energy Lett.*, 2021, **6**, 2499–2501.
- Z. Chen, H. Xue, G. Brocks, P. A. Bobbert and S. Tao, *ACS Energy Lett.*, 2023, **8**, 943–949.
- Y.-R. Wang, A. Senocrate, M. Mladenović, A. Dučinskas, G. Y. Kim, U. Rothlisberger, J. V. Milić, D. Moia, M. Grätzel and J. Maier, *Adv. Energy Mater.*, 2022, **12**, 2200768.
- J. Cho, J. T. DuBose, A. N. T. Le and P. V. Kamat, *ACS Mater. Lett.*, 2020, **2**, 565–570.
- K. Mao, W. Ke, L. Pedesseau, Y. Wu, C. Katan, J. Even, M. R. Wasielewski, C. C. Stoumpos and M. G. Kanatzidis, *J. Am. Chem. Soc.*, 2018, **140**, 3775–3783.
- Y. Li, J. V. Milić, A. Ummadisingu, J.-Y. Seo, J.-H. Im, H.-S. Kim, Y. Liu, M. I. Dar, S. M. Zakeeruddin, P. Wang, A. Hagfeldt and M. Grätzel, *Nano Lett.*, 2018, **19**, 150–157.
- M. C. Gélvez-Rueda, P. Ahlawat, L. Merten, P. Jahanbakhshi, M. Mladenović, A. Hinderhofer, M. I. Dar, Y. Li, A. Dučinskas, B. Carlsen, W. Tress, A. Ummadisingu, S. M. Zakeeruddin, F. Schreiber, A. Hagfeldt, U. Rothlisberger, F. C. Grozema, J. V. Milić and M. Graetzel, *Adv. Funct. Mater.*, 2020, **30**, 2003428.
- A. Dučinskas, G. Y. Kim, D. Moia, A. Senocrate, Y.-R. Wang, M. A. Hope, A. Mishra, D. J. Kubicki, M. Siczek, W. Bury, T. Schneeberger, L. Emsley, J. V. Milić, J. Maier and M. Grätzel, *ACS Energy Lett.*, 2020, **6**, 337–344.
- A. Dučinskas, G. C. Fish, M. A. Hope, L. Merten, D. Moia, A. Hinderhofer, L. C. Carbone, J.-E. Moser, F. Schreiber, J. Maier, J. V. Milić and M. Grätzel, *J. Phys. Chem. Lett.*, 2021, **12**, 10325–10332.
- A. Q. Alanazi, M. H. Almalki, A. Mishra, D. J. Kubicki, Z. Wang, L. Merten, F. T. Eickemeyer, H. Zhang, D. Ren, A. Alyamani, Y. H. Albrithen, A. Albadri, M. H. Alotaibi, A. Hinderhofer, S. M. Zakeeruddin, F. Schreiber, A. Hagfeldt, L. Emsley, J. V. Milić and M. Graetzel, *Adv. Funct. Mater.*, 2021, **31**, 2101163.
- Z. Lai, F. Wang, Y. Meng, X. Bu, X. Kang, Q. Quan, W. Wang, C. Liu, S. Yip and J. C. Ho, *Adv. Opt. Mater.*, 2021, **9**, 2101523.
- C. Lermer, A. Senocrate, I. Moudrakovski, T. Seewald, A.-K. Hatz, P. Mayer, F. Pielnhofer, J. A. Jaser, L. Schmidt-Mende, J. Maier and B. V. Lotsch, *Chem. Mater.*, 2018, **30**, 6289–6297.
- T.-Y. Yang, G. Gregori, N. Pellet, M. Grätzel and J. Maier, *Angew. Chem., Int. Ed.*, 2015, **54**, 7905–7910.
- A. Senocrate, I. Moudrakovski, G. Y. Kim, T.-Y. Yang, G. Gregori, M. Grätzel and J. Maier, *Angew. Chem., Int. Ed.*, 2017, **129**, 7863–7867.



- 33 G. Y. Kim, A. Senocrate, Y.-R. Wang, D. Moia and J. Maier, *Angew. Chem.*, 2021, **133**, 833–839.
- 34 D. Moia, M. Jung, Y.-R. Wang and J. Maier, *Phys. Chem. Chem. Phys.*, 2023, **25**, 13335–13350.
- 35 D. Moia and J. Maier, *ACS Energy Lett.*, 2021, **6**, 1566–1576.
- 36 A. Senocrate, T.-Y. Yang, G. Gregori, G. Y. Kim, M. Grätzel and J. Maier, *Solid State Ionics*, 2018, **321**, 69–74.
- 37 P. V. Kamat and M. Kuno, *Acc. Chem. Res.*, 2021, **54**, 520–531.
- 38 A. Senocrate, T. Acartürk, G. Y. Kim, R. Merkle, U. Starke, M. Grätzel and J. Maier, *J. Mater. Chem. A*, 2018, **6**, 10847–10855.
- 39 A. Senocrate, I. Spanopoulos, N. Zibouche, J. Maier, M. S. Islam and M. G. Kanatzidis, *Chem. Mater.*, 2021, **33**, 719–726.
- 40 A. Senocrate, I. Moudrakovski, T. Acartürk, R. Merkle, G. Y. Kim, U. Starke, M. Grätzel and J. Maier, *J. Phys. Chem. C*, 2018, **122**, 21803–21806.
- 41 M. H. Futscher, J. M. Lee, L. McGovern, L. A. Muscarella, T. Wang, M. I. Haider, A. Fakhruddin, L. Schmidt-Mende and B. Ehrler, *Mater. Horiz.*, 2019, **6**, 1497–1503.
- 42 L. Muscarella, A. Dučinskis, M. Dankl, M. Andrzejewski, N. P. M. Casati, U. Rothlisberger, J. Maier, M. Graetzel, B. Ehrler and J. V. Milić, *Adv. Mater.*, 2022, **34**, 202108720.
- 43 L. McGovern, M. H. Futscher, L. A. Muscarella and B. Ehrler, *J. Phys. Chem. Lett.*, 2020, **11**, 7127–7132.
- 44 B. Conings, J. Drijkoningen, N. Gauquelin, A. Babayigit, J. D’Haen, L. D’Olieslaeger, A. Ethirajan, J. Verbeeck, J. Manca, E. Mosconi, F. D. Angelis and H.-G. Boyen, *Adv. Energy Mater.*, 2015, **5**, 1500477.
- 45 J. Haruyama, K. Sodeyama, L. Han and Y. Tateyama, *J. Am. Chem. Soc.*, 2015, **137**, 10048–10051.
- 46 R. García-Rodríguez, D. Ferdani, S. Pering, P. J. Baker and P. J. Cameron, *J. Mater. Chem. A*, 2019, **7**, 22604–22614.
- 47 S. Meloni, T. Moehl, W. Tress, M. Fccaron, M. Saliba, Y. H. Lee, Y. P. Gao, M. K. Nazeeruddin, S. M. Zakeeruddin, U. Rothlisberger and M. Graetzel, *Nat. Commun.*, 2016, **7**, 10334.
- 48 R. A. D. Souza and D. Barboni, *Chem. Commun.*, 2019, **55**, 1108–1111.
- 49 S. Tan, I. Yavuz, N. De Marco, T. Huang, S.-J. Lee, C. S. Choi, M. Wang, S. Nuryyeva, R. Wang, Y. Zhao, H.-C. Wang, T.-H. Han, B. Dunn, Y. Huang, J.-W. Lee and Y. Yang, *Adv. Mater.*, 2020, **32**, 1906995.
- 50 A. Mahapatra, *Phys. Chem. Chem. Phys.*, 2020, **22**, 11467–11573.
- 51 S. Ahmad, P. Fu, S. Yu, Q. Yang, X. Liu, X. Wang, X. Wang, X. Guo and C. Li, *Joule*, 2019, **3**, 794–806.

